

Potential mechanisms responsible for occurrence of core oxygen minimum zone in the north-eastern Arabian Sea

V.V.S.S. Sarma^{1,2,*}, T.V.S. Udaya Bhaskar³, J. Pavan Kumar³, and Kunal Chakraborty³

¹CSIR-National Institute of Oceanography, Regional Centre,
176 Lawsons Bay Colony, Visakhapatnam – 530 017, India

²Academy of Scientific and Innovative Research,
Dona Paula – 403004, Goa

³Indian National Centre for Ocean Information Services,
Ministry of Earth Sciences (MoES), Pragathi Nagar,
Hyderabad-500090, India

*Corresponding author (sarmav@nio.org)

Abstract

The thickness of oxygen minimum zone (OMZ) is estimated for the first time using dissolved oxygen (DO) profiles obtained from the Biogeochemical Argo floats collected between 2013 and 2019 in the Arabian Sea. The depth of upper boundary of the OMZ varied narrowly between 70 and 220 m in the entire Arabian Sea whereas the lower boundary of OMZ significantly deepened from south (500 m) to northern Arabian Sea (1200 m). The thickness of OMZ decreased from north (>1050 m) to south (400 m) with the thickest OMZ in the northeastern Arabian Sea (950-1050 m). The thick OMZ in the northeastern Arabian Sea is associated with low concentration of depth integrated Chlorophyll-a, primary production in the upper 100 m and sinking carbon fluxes at 100 m depth than other regions. The particle back-scatter, proxy for particulate organic matter, is higher in the northeastern than other regions in the Arabian Sea. The high particle back-scatter data is found in the core of OMZ and it is increased from shelf to offshore indicating that cross-shelf transport of organic matter may be supporting bacterial carbon demand in the OMZ in the northeastern Arabian Sea. The eastward shift in the OMZ is attributed to weak mixing, high penetration time of intermediate water masses, and organic matter transport from the shelf region. Numerical models estimated negligible changes in DO in the OMZ since past several decades, whereas long-term observational data indicates decline in DO levels in the OMZ. Such contrasting results may be caused by lack of cross-shelf transport of organic matter in the models. Though this study identifies the occurrence of cross-shelf transport, the nature, quality and composition of organic matter transported from shelf is unknown. Nevertheless, inclusion of such processes in the models may improve predictability of possible changes in OMZ in future in the Arabian Sea.

1. Introduction

The deoxygenation is one of the most important changes occurring in the marine environment as it will impact marine biodiversity, primary production, trace gases emissions, carbon and nitrogen biogeochemical cycles (Breitburg et al., 2018). The open ocean oxygen minimum zone (OMZ) occurs in many regions in the world ocean such as the Eastern Tropical Pacific (ETP), northern Indian Ocean (Arabian Sea (AS) and Bay of Bengal (BoB)) (Naqvi et al., 1991; Sarma et al., 2016), Eastern Equatorial Pacific (Ruch et al., 2012; Kalvelage et al., 2013; Castro-Gonzalez et al., 2014), and Tropical Atlantic (Levin, 2018), but denitrification is noticed only in the former two basins (eg: Naqvi, 1991;). The denitrification in the Arabian Sea contributes to 8-21% of global marine pelagic denitrification (Naqvi et al., 2006). The main denitrification zone is located in the upper one-third of the OMZ, where O₂ concentrations fall below 0.06 ml/l (~3 μM). This zone is readily identifiable using secondary nitrite maximum due to reduction of NO₃ (Lomas and Lipschultz, 2006).

Despite perennial existence of OMZ, the strong seasonal and interannual variation in concentrations of dissolved oxygen (DO) is reported in the Arabian Sea (Rixen et al., 2014). Recently, Shenoy et al. (2020) found the seasonal variation in the southern boundary of OMZ, which expands down to 9°N during the southwest (SW) monsoon and shrinks to 11°N during the northeast (NE) monsoon. Numerical models suggested expansion of OMZ in the tropical oceans, especially in the Atlantic and Pacific Oceans, in contrast, no substantial changes are noticed in the tropical Indian Ocean since last three decades (Stramma et al., 2008; Breitburg et al., 2018). On the other hand, Banse et al. (2014), based on time-series DO observations, reported annual depletion of DO in the OMZ by 0.19 and 0.08 μM respectively in four decades during NE and SW monsoons respectively between 15° and 20°N but an opposing trend is noticed in the north of 21°N. Lachkar et al. (2018) noticed that intensification of monsoon winds, which is possible due to climate change, enhances primary production leading to expansion of the OMZ in the Arabian Sea. They further noticed that upper region of OMZ is weakened due to ventilation whereas expansion of OMZ is resulted from biological consumption of oxygen.

The occurrence of OMZ in the Arabian Sea is attributed to lack of ventilation from north due to land-locked associating with high primary and export productions resulting in enhanced oxygen consumption (Naqvi, 1991; Stramma et al., 2008; Gilly et al., 2013). The sinking carbon fluxes to OMZ are not sufficient to support bacterial carbon demand (Ducklow et al., 1990; Buesseler et al., 1998; Anand et al., 2018). Naqvi et al. (1993) hypothesized that dissolved organic carbon (DOC), advected from south, may support bacterial carbon demand in the OMZ. The vertical distribution of

DOC does not show any significant gradients in their concentration within OMZ between northeast and northwestern Arabian Sea (Hansell and Peltzer, 1998) indicating that alternative carbon sources may be possible to support bacterial carbon demand in the OMZ. Numerical model simulations suggested that vertical and horizontal mixing governs dissolved oxygen levels in the OMZ on seasonal scale whereas oxygen removal by biological processes are counterbalanced by supply of oxygen by physical processes on annual scale (Sarma, 2002; Resplandy et al., 2012; McCreary et al., 2013; Acharyya and Panigrahi, 2016). Recently, Shenoy et al. (2020) suggested that the balance between oxygen supply by downwelling and advection of oxygen-rich Indian Central Watersmass (ICW) determines the strength of OMZ.

Unlike in Pacific and Atlantic, the core of the OMZ is shifted to low productive northeastern Arabian Sea, which is away from the high productive western boundary upwelling region (Naqvi, 1991). Several hypotheses have been proposed on eastward shift in the core of OMZ in the Arabian Sea. They are 1) advection of oxygen-rich water along the Omani coast in the western Arabian Sea, 2) lack of eddy mixing in the eastern than western Arabian Sea (McCreary et al., 2013; Schmidt et al., 2020b), 3) higher rate of advection of oxygen rich Persian Gulf (PGW) and Red Sea Watermasses (RSW) to the western than eastern Arabian Sea (Schmidt et al., 2020a), 4) horizontal advection of detritus from highly productive western to eastern Arabian Sea (McCreary et al., 2013; Acharyya and Panigrahi, 2016), 5) Intrusion of Indian Central Waters (ICW) from southern boundary and westward propagating Rossby waves radiated off the west coast of India (Shenoy et al., 2020), and 6) cross-shelf transport of organic matter from the eastern continental shelf of Arabian Sea (Somayajuly et al., 1996). Though several hypotheses have been proposed, the northeastward shift in the core of OMZ is still debated (McCreary et al., 2013; Acharya and Panigrahy, 2016; Shenoy et al., 2020).

Despite several decades of research on existence of OMZ in the Arabian Sea, the spatial variability in upper, lower boundaries and thickness of OMZ is unclear due to collection of DO data at the standard depths. Though numerical models showed the variability in thickness of OMZ (eg: Schmidt et al., 2020a and references therein), but these models need validation with ground truth data. Recent development of sensors and high-resolution measurements under Biogeochemical Argo (BGC-Argo) program, significant amount of data has been collected in the Arabian Sea. The objectives of this work is to evaluate 1) spatial variability in upper, lower boundary and thickness of OMZ and processes determining their variability, 2) potential reasons responsible for eastward shift in core of OMZ from the highly productive zone in the western Arabian Sea, and 3) role of cross-shelf transport of organic carbon on eastward shift in core of OMZ.

2. Material and methods

In this study, we have used BGC-Argo profiles of temperature, salinity, dissolved oxygen (DO), fluorescence and back-scatter data collected during different periods between 2013 and 2019 in the Arabian Sea (see for details Table 1). The detailed quality control and data processing of BGC-Argo data are given below.

2.1. Bioargo floats

The floats used are listed in Table 1 along with their bio-optical sensors details. In total 24 floats deployed by the Indian National Centre for Ocean Information Services (INCOIS), National Institute of Oceanography (NIO), and Monterey Bay Aquarium Research Institute (MBARI) are used in this analysis. All the floats were equipped with a CTD, oxygen optode sensor (Aanderaa Optode 4330 sensor) and combined fluorescence/backscattering sensor (SBE/Wetlabs FLBBAP2) measuring fluorescence at 695 nm (with excitation at 470 nm) and optical backscattering at 142° and 700 nm (Table 1). The accuracies of these sensors are 2.4 db, 0.002°C, 0.005 psu, <8 µM, 0.016 µg/L and 0.003 m⁻¹ respectively. All these floats measure data at predetermined depth intervals during ascent. The position of all the profiles used in this study are given in Figure 1.

2.1.1. Temperature and Salinity

Temperature and salinity data were processed and quality-controlled according to the protocol proposed by Argo Data Management Team (Wong et al., 2020). Additional quality control was done to temperature and salinity data following Udaya Bhaskar et al. (2012). The mixed layer depth (MLD) is calculated using a density threshold criterion i.e. the depth at which the density is increased by 0.125 kg m⁻³ compared to the density at 10m (Monterey et al., 1997).

2.1.2. Dissolved Oxygen

Oxygen concentration profiles were derived following the procedures recommended by the BGC-Argo manual (Thierry et al., 2018). All the raw values were converted to oxygen concentration values (µmol kg⁻¹) using the factory calibrations, employing a polynomial fitting equation or based Stern-Volmer equation as per the manuals supplied by the manufacturer. No shipboard oxygen sensor or wet chemical (Winkler) oxygen analyses were available for any of these deployments. Accordingly, these profiles are quality controlled in real time using Thierry and Bittig (2018). Further these profiles are corrected by comparing with world ocean atlas-2018 data following Takeshita et al. (2013). For this correction, SAGE-O2 software developed by MBARI was used and the oxygen data was adjusted. The error estimate in using the climatology for correction of data

comes to 4-6 mbar on partial pressure of oxygen. The overall accuracy of the DO data generates an error on depth of upper and lower boundary of OMZ up to 8-20 m.

2.1.3. Chlorophyll-a

The scale factor (SF) and the dark count (DC) provided by the manufacturer were used to derive Chlorophyll-a (Chl-a) concentrations from fluorescence profiles measured by the float. The following equation is used to convert the counts measured by the float to chl-a concentration:

$$\text{Chl-a} = SF (\text{counts} - DC)$$

The Chl-a data is corrected for non-photochemical quenching (NPQ) and others as suggested by the BGC-Argo Team following Schmechtig et al. (2014). The resultant profiles obtained after these quality control were used to generate the depth integrated Chl-a values. The Chl-a value was integrated from surface to 100 m, which is the mean photic depth in the Arabian Sea (Sarma and Dalabehera, 2019).

2.1.4. Optical backscattering

The volume scattering function $\beta(\lambda, \theta_c)$, at chosen angle θ_c , as measured by the Wetlabs FLBB sensor consists of the backscattering input from particles $\beta_p(\lambda, \theta_c)$ and scattering of light by seawater $\beta_w(\lambda, \theta_c)$. Using the float temperature, salinity data and a depolarization ratio of 0.039, Zhang et al. (2009) calculated the backscattering by seawater at the sensor scattering angle and wave length. Then the total particulate backscattering coefficient from particles at 700 nm, which is generally referred to as b_{bp} , was calculated as:

$$b_{bp}(700) = 2\pi\chi (\beta(700, \theta_c) w(700, \theta_c))$$

where χ is the ratio of the total hemispheric signal to the sensor angle signal. Sullivan et al. (2013) showed this to be relatively constant for marine particles, with $\chi = 1.097$ for $\theta_c = 142^\circ$ (the FLBB sensor angle).

As no ship borne *in situ* data were available to perform post-deployment calibration of sensors, factory calibrations provided by the manufacturer were used. However, in addition to the quality control procedures mentioned above, all the individual profiles were visually checked for the presence of abnormal spikes and any other spurious data points. The BGC-Argo's data can be obtained from (<http://www.coriolis.eu.org/Data-Products/Data-Delivery/Argo-floats-by-WMO-number>) or from the coriolis ftp site (<ftp://ftp.ifremer.fr/ifremer/argo/dac/>).

2.2. Identification of upper, lower boundary and thickness of OMZ

Using the entire BGC-Argo's dissolved oxygen data available in the Arabian Sea, the upper and lower boundary of the OMZ was identified. The depth where DO concentrations dropped to $10\ \mu\text{M}$ from the surface is identified as the upper boundary and the depth where DO concentration increased from $10\ \mu\text{M}$ is identified as depth of lower boundary. The difference between upper and lower boundary is presented as thickness of OMZ.

2.3. Numerical model

The ocean general circulation model used in this study is the ROMS (version 3.7). ROMS is a free-surface, terrain-following, primitive equations ocean model widely used by the scientific community for a diverse range of applications (Song and Haidvogel, 1994; Haidvogel and Beckmann, 1999; Haidvogel et al., 2000; Marchesiello et al., 2003; Shchepetkin and McWilliams, 2003; 2005; Wilkin et al., 2005, Haidvogel et al., 2008; Fennel et al, 2006; 2008; 2013; Chakraborty et al., 2018; 2019a; 2019b). A fully coupled, high resolution regional model has been configured using ROMS for the Indian Ocean (30°E to 120°E ; 30°S to 30°N). The model has a horizontal grid resolution of $1/12^{\circ}$ (approximately 9 km) and uses 40 vertical layers in a terrain-following s-coordinate system. A one-way nested modelling approach is adopted in which a global ocean general circulation model provides boundary data to a regional model that is further coupled with an ecosystem model (Shulman et al., 2004). The Global Ocean Data Assimilation System (GODAS), configured and operationalized at the Indian National Centre for Ocean Information Services (INCOIS) using Modular Ocean Model-4.0 (Ravichandran et al., 2013), has been used to prescribe open boundaries for the Indian Ocean ROMS. The GODAS has $1/2^{\circ}$ resolution in zonal and meridional direction, however the meridional resolution is $1/4^{\circ}$ within 10°S - 10°N and it carries 40 vertical levels.

The Indian Ocean ROMS is spun-up for 30 years from a cold start which is large enough to bring even the slowest moving baroclinic wave to the western boundary and to bring net kinetic energy of a model to a steady state. To begin with, the physical state of the Indian Ocean ROMS is initialized using an initial state derived from the monthly climatological values of January of all the prognostic variables of the physical state of the ocean estimated from the GODAS. The tracers (temperature and salinity) along the eastern and southern open boundary are sponged to monthly climatological values derived from GODAS whereas momentum fluxes are nudged to climatological velocity fields derived from GODAS. The model is forced with NCMRWF's winds, precipitation and radiation fluxes (Prasad et al 2014). The K-Profile Parameterization (KPP; Large et al. 1994) vertical mixing scheme is used for parameterization and biharmonic viscosity and diffusion schemes are chosen for

horizontal mixing (Griffies and Hallberg, 2000). Surface heat and momentum fluxes are internally calculated by ROMS using the bulk parameterizations (Liu et al., 1979; Fairall et al., 1996a; 1996b). The surface salinity is restored to observed climatological values at a relaxation time scale of 1-month.

An inter-annual run of the Indian Ocean ROMS has been carried out from the fully spun up state of the physical state of the ocean from the year 2003 to 2017. The weekly averaged boundary on interannual time scale derived from the GODAS is prescribed for the tracers (i.e. temperature and salinity), sea surface height and momentum fields along the east and south lateral boundary. The multiyear average (2006–2017) of monthly composite of Indian Ocean ROMS simulated velocity fields have been used to study circulation pattern in the upper 300 m of the ocean. The detailed description and validation of the Indian Ocean ROMS model have been presented in Chakraborty et al. (2017; 2018; 2019a; 2019b).

3. Results

3.1. Variations in boundaries and thickness of OMZ in the Arabian Sea

The typical seasonal circulation pattern and unique physical processes are depicted in the Figure 1. Based on the physical features, the Arabian Sea divided into four zones, such as northwest (15-25°N and 50-62°E; NW), northeast (15-25°N; 62-75°E; NE), southwest (5-15°N; 50-62°E; SW) and southeast (5-15°N; 62-75°E; SE) (Fig. 1). The upper boundary of the OMZ varied between 70 and 210 m in the Arabian Sea. The upper boundary of OMZ displayed significant spatial variability with deeper in the SW (150-210 m) followed by NE (130-140 m) than other regions (70-140 m) (Fig. 2a). The shallowest upper boundary of OMZ is observed in the SE (70-130m) Arabian Sea (Fig. 2a). The lower boundary of the OMZ showed significant meridional variability with deeper in the north of 15°N (>1000 m) than south (550-1000 m) (Fig. 2b). The deepest lower boundary was observed in the northeastern Arabian Sea (1050 - 1250 m) followed by northwestern region (900-1200 m). In north of 15°N, significant meridional difference in lower boundary of OMZ is noticed with shallower in the south than northern Arabian Sea (Fig. 2b). There is a clear trend of deepening of lower boundary of OMZ from south to north and such trend is not observed in case of upper boundary (Fig. 2a). The thickness of the OMZ showed significant meridional variability with thinner in the south (400-900 m) and thicker in the north of 15°N (750-1100 m). The thickest OMZ is observed in the northeastern Arabian Sea (950-1100 m) followed by northwestern Arabian Sea (700-1080 m). The spatial variations in the thickness is mainly contributed by the variations in the lower boundary of the OMZ (Fig. 2c).

3.2. Variations in particle back-scatter in the OMZ

The vertical profile of the particle back scattering along the northeast to the southwest transect is plotted in Figure 3a in the upper 500 m. The particle back-scatter varied between 0.0003 and 0.00124 m^{-1} in the upper 500 m (Fig. 3a). The particle back scattering is higher in the upper 50 m of water column and decreased with depth with a prominent subsurface particle maximum between 175 and 400 m centred at 300m, where the core of OMZ situated (Fig. 3a). The subsurface maximum increased from continental margin of northeast coast to the offshore. The tongue like structure is extended towards west up to 63°E, which is the core of OMZ where oxygen concentrations were $<5 \mu\text{M}$ (Fig. 3a). The particle back-scatter showed significant spatial variability at 300 m depth, where core of particle subsurface maximum is observed, with higher in the eastern than western Arabian Sea with clear gradient from shelf to offshore (Fig. 3b). Particle back-scatter is more than twice higher within the core OMZ than outside at 300 m depth in the Arabian Sea and it was decreased from north to south. Though significant gradient in particle back-scatter is noticed between shelf and offshore, however this gradient is more in the north compared to central and southern Arabian Sea (Fig. 3b). Gradual decrease in particle back-scatter from shelf to offshore is noticed in the southern Arabian Sea (Fig. 3b).

3.3. Variations in mixed layer depth and phytoplankton biomass in the upper 100 m

In order to examine the spatial variations in nutrients inputs and phytoplankton biomass in the photic zone, mixed layer depth (MLD) and integrated Chl-a in the upper 100 m is examined. The climatological MLD, computed based on Argo's temperature and salinity profiles, varied between 20 and 70 m with relatively shallow in the eastern than western Arabian Sea (Fig. 4a). Though it was patchy, the mean MLD was lower in the eastern than western Arabian Sea. The depth integrated (column) Chl-a to upper 100 m varied between 40 and 100 mg m^{-2} in the Arabian Sea with significant spatial variations (Fig. 4b). In contrast to MLD, significant zonal gradient in column Chl-a was observed with about 30-40% higher in the west than eastern Arabian Sea. The lower column Chl-a was observed above the core OMZ region than outside associating with shallow MLD (Fig. 4a,b).

3.4. Spatial variations in the speed and direction of currents in the OMZ

The currents at the 300 m depth (core of OMZ) during January and July, that represents the northeast and southwest monsoons respectively, are presented in the Figure 5 with dominant current pattern is depicted with yellow line. The major circulation at 300 m shows dominant westward flow close to the equator during both January and July and it turns to largely cyclonic direction (depicted by

yellow line) in the western Arabian Sea during January and largely anticyclonic direction (depicted by yellow line) during July. Systematic seasonal circulation prevails between equator and 10°N whereas mesoscale eddies are noticed north of 10°N during both January and July (Fig. 5). Equatorward flow is seen in January and it is replaced by poleward flow in July in the western Arabian Sea. The speed of current at 300m was the lowest in the NE followed NW Arabian Sea than other regions. The direction of current does not show systematic pattern in the NE Arabian Sea and shows eddy-kind of structure. The flow is sluggish on the NE side of the seasonal gyres compared to western Arabian Sea (Fig. 5). The spatial variations in temperature, salinity and dissolved oxygen at 300 m, the core of OMZ, in the Arabian Sea suggests that warmer, saltier and low oxygen concentrations are observed in the north of 15°N, and contrasting to that was observed in the in the south of 15°N in the Arabian Sea (Fig. 6).

4. Discussion

4.1. Potential reasons responsible for significant spatial variations in thickness of OMZ

The biogeochemistry of Arabian Sea is governed by seasonally varying different physical mechanisms such as convective mixing, north of 17°N, during winter, coastal upwelling along the Oman, Somalia (eg: Morrison et al., 1999) and southwestern Indian coast (eg: Naqvi et al., 2000) and open ocean upwelling due to findlater jet during summer in the central Arabian Sea (eg: Prasanna Kumar et al., 2001). The currents in the OMZ also change their direction with reference to season (Schott and McCreary, 2001). Seasonal reversal in current direction and vertical mixing at the upper boundary of OMZ are responsible for maintenance of perennial OMZ in the Arabian Sea (Sarma, 2002; Respandy et al., 2012; McCreary et al., 2013; Schmidt et al., 2020b). The variations in the upper and lower boundary of the OMZ are mainly manifested by physical processes in the Arabian Sea. Due to spatial variations in physical processes, the Arabian Sea is divided into four zones, i.e., 1) Northeastern (NE), 2) Northwestern (NW), 3) Southwestern (SW) and 4) Southeastern (SE) Arabian Sea to examine the potential reasons responsible for the variability in thickness of OMZ.

4.1.1. NE Arabian Sea

The typical seasonal circulation at different depth layers are reported by Schott and McCreary (2001) in the Arabian Sea. The circulation within the core of OMZ at 300m depth shows that the weakest currents were observed during northeast (January) and southwest (July) monsoon periods in the NE Arabian Sea compared to other regions. Dominant cyclonic circulation was observed between 12 and 18° N whereas small eddy kind of structures are noticed in the north of 18°N in the NE Arabian Sea (Fig. 5a,b). Meandering flow with weak current speed and eddy kind of structure were observed

during both winter and summer resulting in increase in the ventilation time of water in the NE Arabian Sea.

The thickest OMZ (>500 m) is observed in the NE Arabian Sea, which is mainly caused by deeper lower boundary of OMZ as the depth of upper boundary did not differ significantly from that of west and south (Fig. 2a). The deep lower boundary (1050-1250 m) and thick OMZ (900-1080 m) is noticed in the NE Arabian Sea than other regions (Fig. 2c) associating with sluggish circulation (Fig. 5). Morrison et al. (1999) estimated thickness of the OMZ based on the *in situ* observations during US JGOFS based on the 4.5 μM (0.1 ml/l) boundary and found that ~1000 m close to the Oman coast and <100 m in the south of 15°N with the thickest OMZ in the north of 17°N in the NE Arabian Sea. Schmidt et al. (2020a,b) found that northern Arabian Sea receives low oxygen waters from the north due to long ventilation times and also passage of source water through high productivity area leading to decrease in oxygen concentrations resulting in increase in thickness of the OMZ. Banse et al. (2014) suggested that OMZ in the Arabian Sea is maintained by the balance between the supply of O₂ through eddy mixing and horizontal advection, mainly from the southwest, and O₂ consumption through bacterial activity. Based on numerical modelling, McCreary et al. (2013) reported that the eddy activity is more in the western than eastern Arabian Sea leading to increase in thickness and decrease in oxygen levels in the OMZ in the latter basin.

Madhupratap et al. (1996) found that winter convective mixing, extends down to north of 17°N, leads to the deepening of mixed layer and upward transport of nutrients into the surface waters from the base of the mixed layer. Enhanced nutrient concentrations, for instance nitrate concentrations of >2 μM at the surface, are reported in the northern Arabian Sea due to convective mixing during winter (Madhupratap et al., 1996; de Souza et al., 1996; Morrison et al., 1999). The warmer and saltier waters associated with low oxygen concentrations are observed in the OMZ at the depth of 300 m in the NE compared to other region further indicating that winter convective mixing has significant impact on the thickness of OMZ in the NE region (Fig. 6a-c). Increase in phytoplankton biomass and primary production are reported in response to winter convective mixing (Sawant et al., 1996; Bhattathiri et al., 1996; Barber et al., 2001).

Primary production integrated to the photic zone is less in the NE compared to the NW Arabian Sea (Fig. 7a) and it is consistent with climatological primary production (Qasim, 1982). Similarly, the sinking carbon fluxes from the depth of 100 m are consistent with primary production in the euphotic zone (Fig. 7b; Buesseler et al., 1998; Ramaswamy and Gaye, 2006; Anand et al., 2018). Based on mean primary production and sinking carbon fluxes, about 6±1% of the primary production left the

euphotic zone to the OMZ in the NE Arabian Sea. Anand et al. (2018) reported that about 10% of the mean primary production leaves the euphotic zone in the Arabian Sea and it is higher in the western than eastern basin. Rixen et al. (2019) found that sinking carbon fluxes to the deep Indian Ocean is mainly controlled by the composition of primary producers as dominant opal and carbonates production is observed in the western and eastern Arabian Sea respectively. The density of opal frustules is significantly higher than carbonates (Rixen et al., 2019), the sinking rate of organic matter in the OMZ is low in the NE than NW Arabian Sea. Though fraction of primary production reaches to the OMZ is low (6%) in the NE Arabian Sea, however, more time is available for organic matter to be decomposed within the OMZ due to lower sinking rates associating with carbonates. This would lead to formation of thicker OMZ in the NE Arabian Sea (Fig. 2c). Schmidt et al. (2020a) reported that the supply of oxygen through Persian Gulf (PGW) and Red Sea watermasses (RSW) is not uniform in the OMZ and it is weaker to the eastern Arabian Sea leading to possible to maintain intense OMZ. It was further noticed that the ventilation period is longer for both PGW and RSW in the eastern (2-3 and 7-8 years respectively) than western Arabian Sea (1-2 and 3-4 years respectively; Schmidt et al., 2020a). This result in formation of thicker OMZ in the north eastern than western Arabian Sea. Naqvi et al. (1993) found that sinking carbon fluxes are not enough to support bacterial carbon demand in the OMZ and alternative sources are required in the NE Arabian Sea. Therefore, the occurrence of thick OMZ in the NE Arabian Sea cannot be supported by neither age of the water mass/sluggish circulation nor sinking carbon fluxes. It is hypothesized that external organic matter supply may be supporting high bacterial carbon demand in the OMZ leading to formation of thick OMZ in the NE Arabian Sea.

4.1.2. NW Arabian Sea

The NW Arabian Sea also showed systematic circulation with equatorward flow during winter and poleward flow during summer (Fig. 5). Several eddy-kind of structures are found during winter and summer seasons in the NW Arabian Sea. McCreary et al. (2001) reported that more eddies forms in the western than eastern Arabian Sea. The thicker OMZ (>750 m) is observed in the NW Arabian Sea, however it was not as thick as in the NE Arabian Sea (>950 m). The lower boundary of OMZ is relatively shallower (600-1000 m) in the NW compared to NE Arabian Sea (950-1080 m). Despite high Chl-a and shallow MLD associating with coastal upwelling in the NW Arabian Sea, the upper boundary of the OMZ is relatively deeper by 10-20 m than NE Arabian Sea suggesting that faster sinking of organic organic matter did not remove oxygen from the OMZ (Fig. 2 and 7). The NW Arabian Sea is highly productive due to Oman upwelling (Morrison et al., 1999; Barber et al., 2001) and export production was also observed at 100 m depth in the western than eastern Arabian Sea

(Fig. 7a,b; Buesseler et al., 1998; Barber et al., 2001; Ramaswamy and Gaye, 2006; Anand et al., 2018). Based on the mean primary production in the photic zone and export production at 100 m, it is estimated that about 10% of the primary production in the photic zone reaches to the OMZ in the NW Arabian Sea, which is almost double to that of in the NE Arabian Sea (6%). Rixen et al. (2019) noticed that dominant opal production in the western Arabian Sea leading to faster sinking of carbon to depth as the density of opal frustules is significantly higher than carbonates. As a result, the residence time of sinking carbon is less leading to low decomposition of organic matter in the water column in the NW Arabian Sea. In addition to this high supply of oxygen through Persian Gulf (PGW) and Red Sea watermasses (RSW) is noticed in the western than eastern Arabian Sea with low ventilation period (1-2 and 3-4 years respectively in the western and eastern basins; Schmidt et al., 2020a). Therefore, relatively weaker and thinner OMZ in the NW Arabian Sea is caused by supply of oxygen through eddy pumping and water masses (PGW and RSW) and less modification of sinking carbon fluxes due to faster sinking rates associating with dominant opal contribution.

4.1.3. SE Arabian Sea

The thickness of OMZ in the SE Arabian Sea ranged between 400 and 850 m, and it is less thick than in the northern Arabian Sea. The SE Arabian Sea experiences strong seasonal coastal upwelling leading to the formation seasonal hypoxia (Gupta et al., 2016; Shenoy et al., 2020 and references therein). This region is characterized by high seasonal primary production (Gauns et al., 2005), especially during summer monsoon, lower sinking carbon fluxes (Fig. 7b) and sluggish circulation (Fig. 5). Ramaswamy and Gaye (2006) noticed that planktonic foraminiferal carbonate fluxes are the major contributors to biogenic fluxes in the eastern Arabian Sea. Due to low density of the carbonate (calcite) than opal, the flux of carbon to the deep sea is lower. This result in consumption of most of the organic matter within OMZ leading to less carbon is exported to the deep sea and formation of thick OMZ in the SE Arabian Sea. Recently Shenoy et al. (2020) proposed that mixing of oxygen rich Indian Central watermass (ICW) with OMZ through Rossby waves can potentially influence oxygen levels in the OMZ in the SE Arabian Sea. They further proved that more oxygen is supplied through ICW during upwelling period, when supply of oxygen from surface is limited, but the supply by ICW will be limited when downwelling supplies oxygen from surface to OMZ. The balance between oxygen supply through vertical and horizontal mixing controls the oxygen levels in the OMZ in the eastern Arabian Sea (Acharyya and Panigrahi, 2016; Shenoy et al., 2020).

4.1.4. SW Arabian Sea

The uniform and systematic flows in the south of 12°N is observed with dominant westward or

southwestward flow during both winter (January) and summer (July) seasons and the flow turns to anticyclonic direction in the SW Arabian Sea, off Somalia, during former and cyclonic direction during latter season (Fig. 5). The SW Arabian Sea houses thin OMZ between depth of 420 and 800 m compared to other regions of the Arabian Sea (Fig. 2c). The highest primary production (Barber et al., 2001) and sinking carbon fluxes (Fig. 7a,b) are observed in the SW Arabian Sea due to horizontal advection of nutrient-rich waters from Oman upwelling. Despite high production, and sinking carbon fluxes to bottom, the thickness of OMZ is low that possibly due to faster sinking of organic matter and circulation. Schmidt et al. (2020a) noticed that ventilation time of PGW and RSW is lower in the western than eastern Arabian Sea leading more oxygen in the OMZ in the former than latter. In addition to this, dominant contribution of diatom opal and foramineferal carbonate in this region (Ramaswamy and Gaye, 2006) resulting in faster removal of organic matter from the water column to depth resulting in less modification within the water column before it reaches to the bottom. This would result in higher oxygen levels in the water column and weak OMZ in the SW Arabian Sea. Therefore, the weaker OMZ in the SW Arabian Sea is caused by both faster sinking organic matter and rapid circulation of waters.

4.2. Potential reasons for occurrence of core OMZ and denitrification in the northeastern Arabian Sea

The thickness of OMZ showed significant east-west gradient with thicker in the east of 62°E than western Arabian Sea at a given latitude. Naqvi (1991) reported that subsurface nitrite, as indicator of denitrification, occurs in the NE Arabian Sea, north of 12°N, in the depth range of 200-700 m with core at 300 m and it was absent in the NW Arabian Sea. Occurrence of denitrification does not relate to the primary production in the photic zone as primary production was low in the NE than NW but higher than in the southern Arabian Sea (Fig. 7a) and it is consistent with earlier reports (Qasim et al., 1982; Naqvi 1991). The eastward shift in core OMZ and denitrification is reported to be caused by 1) strong vertical eddy mixing in the west than east resulting in injection of oxygen to the OMZ in the former than latter 2) supply of detritus from highly productive western to eastern Arabian Sea (McCreary et al., 2013), 3) long intermediate watermass (PGW, RSW) ventilation period in the east than western Arabian Sea (Schmidt et al., 2020a), 4) modification in source of DO by ICW associated with Rossby waves (Shenoy et al., 2020), and 5) high oxygen supply through horizontal advection to the western than eastern Arabian Sea at intermediate water depth (Acharya and Panigrahy et al., 2016). In addition to this low residence time of waters due to faster circulation further help to oxidize OMZ waters and inhibit denitrification in the northwestern Arabian Sea (Fig 5). Nevertheless, the dominant mechanism responsible for eastward shift in denitrification is still

well debated.

In addition to physical processes, the rate of sinking fluxes also modifies the magnitude of organic matter reaches to the OMZ as the decomposition of organic matter intensify OMZ. The seasonal mean sinking carbon fluxes at 100 m depth (upper boundary of OMZ) are the highest in the western Arabian Sea, off Oman coast, ($102.7 \pm 41 \text{ mgC m}^{-2} \text{ d}^{-1}$) due to upwelling of subsurface waters followed by NE ($52.6 \pm 34 \text{ mgC m}^{-2} \text{ d}^{-1}$) and the lowest fluxes are noticed in the southern Arabian Sea ($46.9 \pm 20 \text{ mgC m}^{-2} \text{ d}^{-1}$; Fig. 7b; Buessler et al., 1998; Anand et al., 2018). Faster sinking carbon fluxes are reported in the NW Arabian Sea associating with dominant opal production than NE Arabian Sea, where dominant carbonate production is recorded (Ramaswamy and Gaye, 2006). The east-west difference in sinking carbon fluxes may not be responsible for eastward shift in OMZ as Naqvi et al. (1996) estimated that sinking carbon fluxes are not enough to support bacterial carbon demand in the OMZ in the NE Arabian Sea. Therefore, alternative sources of carbon are required to support bacterial carbon demand in the denitrification zone. Naqvi et al. (1993) found existence of nepheloid layers in the core of OMZ (at 300 m) and it was attributed to higher abundance of denitrifying bacteria. Somayajulu et al. (1996) estimated that significant amount of dissolved organic matter advects from the organic matter-rich and anoxic sediments from the continental margins using radium isotopes, however, no evidences have been reported to support this study. In order examine the possible source of particulate organic matter to the OMZ, the particle back-scatter distribution is studied in the Arabian Sea.

4.3. *Cross-shelf transport of particulate organic matter to the OMZ in the northeastern Arabian Sea*

The particle back-scatter is found to linearly correlate with particulate organic carbon (POC) and it can be used as a proxy for POC (Stramski et al., 2008; Cetinic et al., 2012; Rasse et al., 2017). The particle back-scatter is the highest within the denitrification layer suggesting that higher concentration of POC is present in the OMZ in the NE than western Arabian Sea. Low phytoplankton biomass (Fig. 3b), primary production (Fig. 7a), and moderately high sinking carbon fluxes (Fig. 7b) do not support high POC sourced from *in situ* processes alone in the OMZ in the NE Arabian Sea. The vertical distribution of particle back-scatter shows existence of subsurface maxima between 175 and 400 m with high in the core of OMZ at 300 m in the NE Arabian Sea and it is decreased towards western Arabian Sea (Fig. 3a). The intensity of the particle back-scatter decreased from shelf to offshore indicating the possible source from continental margin. The spatial distribution of particle back-scatter at 300m depth also shows higher in the shelf and decreased towards offshore clearly indicating that offshore advection of shelf sediments may supply organic carbon to the denitrification zone in the northeastern Arabian Sea (Fig.3b). This is consistent with Somayajulu et

al. (1996), who reported that, based on radium activity, horizontal advection of organic carbon-rich and deeply anoxic sediments from continental margin sediments at 300 m depth support organic carbon demand in the denitrification layer. Shenoy et al. (2020) reported that the concentration of DO in the OMZ is controlled by horizontal transport of oxygen by baroclinic Rossby waves generated along the west coast of India. Such baroclinic Rossby waves can influence water column up to 500 m. It is, therefore, possible that organic rich particles from the western continental shelf may be brought to the NE Arabian Sea and its consumption through bacterial activity may result in occurrence of intense OMZ. Recently existence of back-scatter maxima in the OMZ region is reported in the Arabian Sea (Wojtasiewicz et al. (2018) and eastern equatorial south Pacific (Ulloa et al., 2012). Wojtasiewicz et al. (2018) noticed significant linear relationship between back-scatter and nitrate deficit and suggested that backscatter may be a useful tracer to denitrification in the Arabian Sea. Nevertheless, this study suggested that occurrence of core OMZ in the northern Arabian Sea may be supported by physical processes, such as water masses, eddies, transport of detritus from the west, ICW and low sinking carbon fluxes, however, the role of cross-shelf transport of organic matter cannot be neglected. Numerical models mostly concentrate on balance of oxygen in the OMZ through physical processes however, the cross-shelf transport of organic matter and role of composition of sinking fluxes are never considered. Though existence of particle maxima is noticed in the core of OMZ, , the nature, quality and composition of particles present in the OMZ, and their utilization by the anaerobic microbial community needs to be evaluated to understand their role on intensifying OMZ in the NE Arabian Sea. Since significant amount of particle back scatter data is being generated through BGC-Argo's program, these data should be converted in terms of organic matter by calibrating particle back scatter data with particulate organic matter. These data should be incorporated in the models to improve our understanding on development of OMZ and prediction of changes in future due to climate change in the in the Arabian Sea.

4.4. Possible changes of intensity of OMZ due to climate change

Banse et al. (2014) found that marked seasonality in oxygen concentrations OMZ with higher oxygen concentrations by 3.5 μM during northeast and spring intermonsoon than southwest monsoon. The mean annual decrease in oxygen levels during northeast and southwest monsoon seasons are -0.2 and -0.08 μM respectively. The decreasing trend is observed between 15 and 20°N and opposite trend is noticed north of 21°N. The diapycnal mixing is more responsible for oxygen supply to OMZ at upper layer of the OMZ (200 m) whereas isopycnal mixing is more responsible at deeper depths (300-500 m) (Sarma, 2002; Resplandy et al., 2012; McCreary et al., 2013; Acharya and Panigrahy, 2016). The rapid warming of Indian Ocean, including Arabian Sea is reported in the

recent decades (Roxy et al., 2015) leading to decrease in primary production (Roxy et al., 2016). Though rapid warming may decrease vertical mixing and solubility of gas in the water resulting in less supply of oxygen to the OMZ leading to intensification of OMZ. In contrast, the decrease in primary production, therefore export production, may decrease oxygen demand in the OMZ. If the changes in dissolved oxygen in the OMZ due to weakening of vertical mixing, low solubility and less export production is balanced, the net impact on OMZ due to climate change may be negligible. Numerical models also simulated insignificant changes in OMZ in the northern Indian Ocean since past 5 decades (Stramma et al., 2008; Breitburg et al., 2018), indicating that possible changes in OMZ may be unlikely due to climate change. However, these models do not include cross-shelf transport of organic matter from the west coast of India, impact of variability in advection of shelf sediments by Rossby waves to the OMZ and modifications in phytoplankton composition thereby changes in sinking carbon flux that significantly influences intensity of OMZ. Therefore, the long-term trends obtained from the numerical models (Stramma et al., 2008; Breitburg et al., 2018) may need further evaluation in the light of cross-shelf transport, size and nature of organic matter sinking to examine the actual long-term trends in the OMZ.

5. Summary and Conclusions

The existence of OMZ is known in the Arabian Sea for more than 6 decades however the spatial variability in its exact thickness is unclear due to lack of availability of fine vertical resolution data. Since last decade, vertical oxygen profiles at high vertical and spatial resolution are available from BGC-Argos program. Based on the data collected between 2013 and 2019, the climatology of the thickness of OMZ is estimated. The thickness of OMZ increased from south (400-750m) to north (950-1080 m) with the thickest OMZ in the northeastern (NE) Arabian Sea (650-950 m), where denitrification is reported. Column (100m) integrated Chlorophyll-a and primary production, sinking carbon fluxes at 100m are low in the east compared to western Arabian Sea indicating that alternative source of organic matter may be possible to support high bacterial carbon demand in the NE Arabian Sea. The weak spatial variations in the upper boundary of OMZ suggest that horizontal advection is more important on intensity of OMZ than vertical mixing. The particle back-scatter, a proxy for particulate organic matter, shows higher signal in the core of OMZ in the NE Arabian Sea with significant gradient between shelf and offshore suggesting that cross-shelf transport of organic-rich sediments from the continental margin seems to support high carbon demand in the OMZ. The existence of core OMZ in the NE Arabian Sea may be caused by weak advection of watermasses (PGW, RSW, ICW), weak eddy mixing in the east and transport of detritus from high productive upwelling region in the west to east and cross-shelf transport of organic matter from eastern

continental margin. Insignificant changes in DO levels in the OMZ is estimated using numerical models whereas decline in oxygen levels are noticed based on long-term data. The discrepancy between observations and models may be due to lack of cross-shelf transport of organic matter, phytoplankton composition and sinking carbon fluxes in the numerical models and prediction may be improved by including such processes. Though significant amount of back-scatter data are available from BGC-Argo program in the Arabian Sea, the quality, nature and composition of organic matter and bacterial utilization rates need to be evaluated before it is incorporated into the models for better prediction of changes in OMZ in the Arabian Sea.

Acknowledgements:

We would like to thank all the Scientists, Technicians and groups involved in the Indian Ocean BGC-Argo's program for making available the data for this work. We would like to thank the Director, NIO and Director, INCOIS for their unconditional support. This work was funded by INCOIS through O-MASCOT program entitled "Influence of anticyclonic eddies on oxygen minimum zone and carbon sequestration". We would like to thank two anonymous reviewers for their constructive suggestions for improvement of presentation of results. This has NIO contribution number.....and INCOIS contribution number ***

Table 1: The details of the BGC-Argofloats used in this study including the identification of float, manufacturer, sensor type, calibration type, beginning and end date of data collected by each float.

WMOID	Manufacturer	O2 sensor type	O2 sensor serial #	O2 calibration type	FLBB sensor type	FFBB serial number	Start Date	End Date
2902091	NKE, France	Optode 4330	1125	Polynomial	Wetlabs AP2	2662	23-FEB-2013	15-MAR-2013
2902092	NKE, France	Optode 4330	718	Polynomial	Wetlabs AP2	2659	24-FEB-2013	14-DEC-2016
2902093	NKE, France	Optode 4330	710	Polynomial	Wetlabs AP2	2661	25-FEB-2013	13-APR-2019
2902118	NKE, France	Optode 4330	1329	Polynomial	Wetlabs AP2	3065	23-FEB-2013	15-MAR-2013
2902120	NKE, France	Optode 4330	1331	Polynomial	Wetlabs AP2	3066	10-MAR-2014	13-MAY-2019
2902123	NKE, France	Optode 4330	1336	Polynomial	Wetlabs AP2	3088	10-MAR-2014	13-MAY-2019
2902124	NKE, France	Optode 4330	1337	Polynomial	Wetlabs AP2	3089	11-MAR-2014	11-OCT-2017
2902156	Teledyne, USA	Optode 4330	1621	Polynomial	Wetlabs AP2	3503	01-DEC-2014	10-JUN-2018
2902174	Teledyne, USA	Optode 4330	1629	Polynomial	Wetlabs AP2	3170	18-FEB-2015	18-MAY-2019
2902175	Teledyne, USA	Optode 4330	1628	Polynomial	Wetlabs AP2	3167	20-FEB-2015	18-MAY-2019
2902179	Teledyne, USA	Optode 4330	1681	Stern-Volmer	Wetlabs AP2	4026	28-AUG-2015	17-MAY-2019
2902199	Teledyne, USA	Optode 4330	1459	Stern-Volmer	Wetlabs AP2	4073	06-MAR-2016	04-JUN-2017
2902202	Teledyne, USA	Optode 4330	1458	Stern-Volmer	Wetlabs AP2	4072	07-MAR-2016	04-JUN-2017
2902204	Teledyne, USA	Optode 4330	1457	Stern-Volmer	Wetlabs AP2	4071	08-MAR-2016	18-MAY-2019
2902205	Teledyne, USA	Optode 4330	1456	Stern-Volmer	Wetlabs AP2	4070	09-MAR-2016	18-MAY-2019
2902110	Teledyne, USA	Optode 4330	1529	Stern-Volmer	Wetlabs AP2	4328	01-OCT-2016	18-MAY-2019
2902111	Teledyne, USA	Optode 4330	1528	Stern-Volmer	Wetlabs AP2	4314	05-OCT-2016	18-MAY-2019
2902116	Teledyne, USA	Optode 4330	1677	Stern-Volmer	Wetlabs AP2	4075	11-DEC-2016	06-APR-2019
2902238	NKE, France	Optode 4330	2657	Stern-Volmer	Wetlabs AP2	4718	23-OCT-2017	18-MAY-2019
2902239	NKE, France	Optode 4330	2661	Stern-Volmer	Wetlabs AP2	4719	26-OCT-2017	20-MAY-2019
2902243	NKE, France	Optode 4330	2721	Stern-Volmer	Wetlabs AP2	4724	06-NOV-2017	17-MAY-2019
2902244	NKE, France	Optode 4330	2738	Stern-Volmer	Wetlabs AP2	4725	06-NOV-2017	17-MAY-2019
2902263	NKE, France	Optode 4330	2783	Stern-Volmer	Wetlabs AP2	4727	27-JAN-2018	19-MAY-2019
5903586	Teledyne, USA	Optode 4330	1333	Polynomial	Wetlabs AP2	2101	06-FEB-2012	14-AUG-2014

References

- Acharya, S.S. and Panigrahi, M.K. 2016. Eastward shift and maintenance of Arabian Sea oxygen minimum zone: Understanding the paradox. *Deep-Sea. Res. I*, 115, 240-252.
- Anand, S.S., Rengarajn, R., and Sarma, V.V.S.S. 2018. ²³⁴Th based carbon export flux along the Indian GEOTRACES GI02 section in the Arabian Sea and the Indian Ocean. *Global Biogeochem. Cycles.*, 32, 417-436.
- Banse, K., Naqvi, S.W.A., Narvekar, P.V., Postel, J.R., and Jayakumar, D.A. 2014. Oxygen minimum zone of the open Arabian Sea: variability of oxygen and nitrite from daily to decadal time scales. *Biogeosciences*, 11, 2237-2261.
- Barber, R. T., Marra, J., Bidigare, R. C., Codispoti, L. A., Halpern, D., Johnson, Z., et al. (2001). Primary productivity and its regulation in the Arabian Sea during 1995. *Deep Sea Research, Part II*, 48(6-7), 1127–1172. [https://doi.org/10.1016/S0967-0645\(00\)00134-X](https://doi.org/10.1016/S0967-0645(00)00134-X)
- Bhattathiri, P. M. A., Pant, A., Sawant, S. S., Gauns, M., Matondkar, S. G. P., & Mahanraju, R. (1996). Phytoplankton production and chlorophyll distribution in the eastern and central Arabian Sea in 1994–1995. *Current Science*, 71(11), 857–862.
- Breitburg, D., Levin, L., Oschlies, A., Gregoire, M., Chavez, F., Conley, D., et al. 2018. Declining oxygen in the global ocean and coastal waters. *Science*, 359, 6371: doi: 10.1126/ science.aam7240.
- Buesseler, K., Ball, L., Andrews, J., Benitez-Nelson, C., Belostock, R., Chai, F., & Chao, Y. (1998). Upper ocean export of particulate organic carbon in the Arabian Sea derived from thorium-234. *Deep Sea Research, Part II*, 45(10-11), 2461–2487.
- Castro-González, M., Molina, V., Rodríguez-Rubio, E. and Ulloa, O. 2014. The first report of a microdiverse anammox bacteria community in waters of Colombian Pacific, a transition area between prominent oxygen minimum zones of the eastern tropical Pacific. *Environm. Microbiol. Rep.*, 6(6): 595-604
- Cetinic, I., et al., 2012. Particulate organic carbon and inherent optical properties during 2008 North Atlantic bloom experiment. *J. Geophys. Res.*, 117, C06028.
- Chakraborty, K., Kumar, N., & Gupta, G. V. M. 2017. Getting the right wind-forcing for an ecosystem model: A case study from the eastern Arabian Sea. *Journal of Operational Oceanography*, 10(2), 176-190.
- Chakraborty, K., K. Valsala, V., Gupta, G. V. M., and Sarma, V. V. S. S. 2018. Dominant biological control over upwelling on pCO₂ in sea east of Sri Lanka. *Journal of Geophysical Research: Biogeosciences*. <https://doi.org/10.1029/2018JG004446>.
- Chakraborty, K., Lotliker, A. A., Majumder, S., Samanta, A., Baliarsingh, S. K., Ghosh, J., Madhuri PP, Saravanakumar A, Sarma NS, Rao BS, Shanmugam P. (2019a). Assessment of model-simulated upper ocean biogeochemical dynamics of the Bay of Bengal. *Journal of Sea Research*, 146, 63-76.
- Chakraborty, K., Kumar, N., Girishkumar, M. S., Gupta, G. V. M., Ghosh, J., UdayaBhaskar, T. V. S., & Thangaprakash, V. P. (2019b). Assessment of the impact of spatial resolution on ROMS simulated upper-ocean biogeochemistry of the Arabian Sea from an operational perspective. *Journal of Operational Oceanography*, 1-27.

- de Souza, S.N., Kumar, M.D., Sardessai, S., Sarma, V.V.S.S. and Shrodkar, P.V., 1996. Seasonal variability in oxygen and nutrients in the central and eastern Arabian Sea. *Curr. Sci.*, 71 (11), 847-851.
- Fairall, C.W., Bradley, E.F., Rogers D.P., Edson J.B and Young G.S. 1996a. Bulk parameterization of air-sea fluxes for tropical ocean global atmosphere Coupled-Ocean Atmosphere Response Experiment, *J. Geophys. Res.*, 101, 3747-3764.
- Fairall, C. W., Bradley, E. F., Godfrey, J. S., Wick, G. A., Edson, J. B., and Young, G. S. 1996b. Cool-skin and warm-layer effects on sea surface temperature. *Journal of Geophysical Research: Oceans*, 101(C1), 1295-1308.
- Fennel, K., Wilkin, J., Levin, J., Moisan, J., O'Reilly, J., &Haidvogel, D. 2006. Nitrogen cycling in the Middle Atlantic Bight: Results from a three-dimensional model and implications for the North Atlantic nitrogen budget. *Global Biogeochemical Cycles*, 20(3).
- Fennel, K., Wilkin, J., Previdi, M., &Najjar, R. 2008. Denitrification effects on air-sea CO₂ flux in the coastal ocean: Simulations for the northwest North Atlantic. *Geophysical Research Letters*, 35(24)..
- Fennel, K., Hu, J., Laurent, A., Marta-Almeida, M., &Hetland, R. 2013. Sensitivity of hypoxia predictions for the northern Gulf of Mexico to sediment oxygen consumption and model nesting. *Journal of Geophysical Research: Oceans*, 118(2), 990-1002.
- Gauns, M., Madhupratap, M., Ramaiah, N., Jyothibabu, R., Fernands, V., Paul, J. T., & Kumar, S. P. (2005). Comparative accounts of biological productivity characteristics and estimates of carbon fluxes in the Arabian Sea and the Bay of Bengal. *Deep Sea Research, Part II*, 52(14-15), 2003–2017. <https://doi.org/10.1016/j.dsr2.2005.05.009>
- Gilly, W.F., Beman, J.M., Litvin, S.Y., and Robison, B.H. 2013. Oceanographic and biological effects of shoaling of the oxygen minimum zone. *Annual Review Mar. Sci.*, 5, 393-420.
- Griffies, S. M., and Hallberg R.W .(2000). Biharmonic friction with a smagorinsky-like viscosity for use in large-scale eddy-permitting ocean models, *Monthly Weather Review*, 128(8), 2935–2946.
- Gupta, G.V.M., Sudheesh, V., Sudharma, K.V., Saravanane, N., Dhanya, V., Dhanya, K.R., Lakshmi, G., Sudhakar, M., Naqvi, S.W.A. 2016. Evolution to decay of upwelling and associated biogeochemistry over the southeastern Arabian Sea shelf. *J. Geophys. Res. Biogeosciences*, 121, 159-175.
- Hansell, D.A., and Peltzer, E.T. 1998. Spatial and temporal variations of total organic carbon in the Arabian Sea. *Deep-Sea Res, II*, 45, 2171-2193.
- Haidvogel, D. B., and Beckmann, A .1999. *Numerical Ocean Modelling*, 330 pp., Imperial Coll. Press, London, UK.
- Haidvogel, D. B., Arango, H. G., Hedstrom, K., Beckmann, A., Malanotte-Rizzoli, P., and Shchepetkin, A. F. 2000. Model evaluation experiments in the North Atlantic Basin: simulations in nonlinear terrain-following coordinates. *Dynamics of atmospheres and oceans*, 32(3-4), 239-281.

- Haidvogel, D. B., Arango, H., Budgell, W. P., Cornuelle, B. D., Curchitser, E., Di Lorenzo, E. and Levin, J. 2008. Ocean forecasting in terrain-following coordinates: Formulation and skill assessment of the Regional Ocean Modeling System. *Journal of Computational Physics*, 227(7), 3595-3624.
- Kalvelage, T., Lavik, G., Lam, P., Contreras, S., Arteaga, L., Loscher, C.R., Oschlies, A., Paulmier, A., Stramma, L., Kuypers, M.M.M. 2013. Nitrogen cycling driven by organic matter export in the South Pacific oxygen minimum zone. *Nature Geosciences.*, 6, 228-234.
- Lachkar, Z., Levy, M., and Smith, S. 2018. Intensification and deepening of the Arabian Sea oxygen minimum zone in response to increase in Indian monsoon wind intensity. *Biogeosciences*, 15, 159-186.
- Large, W.G., McWilliams J.C., and Doney S.C . (1994). Oceanic vertical mixing: A review and a model with a nonlocal boundary layer parameterization. *Reviews of Geophysics* 32: 363–403.
- Levin, L.A. 2018. Manifestation, drivers, and emergence of open ocean deoxygenation. *Annual Review Mar. Sci.*, 10, 229-260.
- Liu, W.T., Katsaros K.B, and Businger J.A, (1979). Bulk parameterization of the air-sea exchange of heat and water vapor including the molecular constraints at the interface, *J. Atmos. Sci.*, 36, 1722-1735.
- Lomas, M.W., and Lipschultz, F. 2006. Forming the primary nitrite maximum: Nitrifiers or phytoplankton? *Limnology and Oceanography*, 51, 2453-2467.
- Madhupratap, M., Kumar, S. P., Bhattathiri, P. M. A., Kumar, M. D., Raghukumar, S., Nair, K. K. C., & Ramaiah, N. (1996). Mechanisms of the biological response to winter cooling in the northeastern Arabian Sea. *Nature*, 384(6609), 349–352.
- Marchesiello, P., McWilliams, J. C., & Shchepetkin, A. (2003). Equilibrium structure and dynamics of the California Current System. *Journal of physical Oceanography*, 33(4), 753-783.
- McCreary, J. P., Yu, Z., Hood, R. R., Vinayachandran, P., Furue, R., Ishida, A. and Richards. K. J., 2013. Dynamics of the Indian-Ocean oxygen minimum zones, *Prog. Oceanogr.*, 112, 15–37.
- Monterey, G. and Levitus, S., 1997: Seasonal Variability of Mixed Layer Depth for the World Ocean. NOAA Atlas NESDIS 14, U.S. Gov. Printing Office, Wash., D.C., 96 pp. 87 figs.
- Morrison, J.M., Codispoti, L.A., Smith, S.L., Wishner, K., Flagg, C., Gardner, W.D., Gaurin, S., Naqvi, S.W.A., Manghnani, V., Prosperie, L., and Gundersen, J.S. 1999. The oxygen minimum zone in the Arabian Sea during 1995. *Deep-Sea Res.*, II, 46, 1903-1931.
- Naqvi, S.W.A., 1991. Geographical extent of denitrification in the Arabian Sea in relation to some physical processes. *Oceanol. Acta.*, 14, 281-290.
- Naqvi, S.W.A., Kumar, M.D., Narvekar, P.V., de Souza, S.N., George, M.D. and D'Silva, C.D., 1993. An intermediate nepheloid layer associated with high microbial metabolic rates and denitrification in the northwest Indian Ocean. *J. Geophys. Res.*, 98 (C9), 16469-16479.
- Naqvi, S.W.A., Jayakumar, D.A., Narvekar, P.V., Naik, H., Sarma, V.V.S.S., D'Souza, W., Joseph, S., and George, M.D. 2000. Increased marine production of N₂O due to intensifying anoxia on the Indian continental shelf. *Nature*, 408, 346-349.

Naqvi, S. W. A., Naik, H., Pratihary, A., D' Souza, W., Narvekar, P. V., Jayakumar, D. A., Devol, A. H., Yoshinari, T. and Saino, T.: Coastal versus open-ocean denitrification in the Arabian Sea, *Biogeosciences Discussions*, 3 (3), 665– 695, doi:10.5194/bgd-3-665-2006, 2006.

Prasad, V., Mohandas, S., Dutta, S. K., Gupta, M. D., Iyengar, G., Rajagopal, E., and Basu, S. (2014). Improvements in medium range weather forecasting system of india. *Journal of earth system science*, 123(2):247–258

Prasanna Kumar, S., Madhupratap, M., Kumar, M.D., Muraleedharan, P.M., Souza, S.N., Gauns, M., and Sarma, V.V.S.S. 2001. High biological productivity in the central Arabian Sea during the summer monsoon driven by Ekman pumping and lateral advection, *Curr. Sci.*, 81, 1633-1638.

Qasim, S. Z. (1982). Oceanography of the northern Arabian Sea. *Deep Sea Research*, 29(9), 1041–1068. [https://doi.org/10.1016/0198-0149\(82\)90027-9](https://doi.org/10.1016/0198-0149(82)90027-9)

Ramaswamy, V., and Gaye, B. 2006. Regional variations in the fluxes of foraminifera carbonate, coccolithophorid carbonate and biogenic opal in the northern Indian Ocean. *Deep-Sea Res. I*, 53, 271-293.

Rasse, R. et al., 2017. Evaluating optical proxies of particulate organic carbon across the surface Atlantic Ocean. *Front. Mar. Sci.*, 4, 367.

Ravichandran, M., Behringer, D., Sivareddy, S., Girishkumar, M.S., Chacko, N and Harikumar, R. 2013. Evaluation of the global ocean data assimilation system at INCOIS: The Tropical Indian Ocean. *Ocean Modelling* 69: 123–135.

Resplandy, L., Lévy, M., Bopp, L., Echevin, V., Pous, S., Sarma, V. V. S. S., and Kumar, D. (2012). Controlling factors of the oxygen balance in the Arabian Sea's OMZ. *Biogeosciences*, 9(12), 5095–5109. doi: 10.5194/bg-9-5095-2012

Rixen, T., Gaye, B., Emels, K.C., Ramaswamy, V. 2019. The ballast effect of lithogenic matter and its influences on the carbon fluxes in the Indian Ocean. *Biogeosciences*, 16, 485-503.

Rixen, T., Baum, A. Gaye, B. and Nagel, B. 2014. Seasonal and interannual variations in the nitrogen cycle in the Arabian Sea. *Biogeosciences*, 11, 5733 – 5747

Roxy, M.K., Ritika, K., Terray, P., Murtugudde, R., Ashok, K., Goswami, B.N. 2015. Drying of Indian subcontinent by rapid Indian Ocean warming and a weakening land-sea thermal gradient, *Nature Communications*, 6, 7423 doi: 10.1038/ncomms8423.

Roxy, M.K., Modi, A., Murtugudde, R., Valsala, V., Panickal, S., Prasanna Kumar, S., Ravichandran, M., Vichi, M., Levy, M. 2016. A reduction in marine primary productivity driven by rapid warming over the tropical Indian Ocean. *Geophys. Res. Lettrs.*, 43, 826-833.

Sarma, V.: An evaluation of physical and biogeochemical processes regulating perennial suboxic conditions in the water column of the Arabian Sea, *Global Biogeochem. Cy.*, 16 (4), 1082, doi:10.1029/2001GB001461, 2002.

Sarma, V.V.S.S., and Dalabehera, H.B. 2019. New and primary production in the western Indian Ocean during fall monsoon. *Mar. Chem.*, 215, 103687, doi: 10.1016/j.marchem.2019.103687.

- Sawant, S., & Madhupratap, M. (1996). Seasonality and composition of phytoplankton in the Arabian Sea. *Current Science*, 71(11), 869–873.
- Schmidt, H., Czeschel, R., Visbeck, M. 2020a. Ventilation dynamics of oxygen minimum zone in the Arabian Sea. *Biogeosciences Discuss*, doi: 10.5194/bg-2019-168.
- Schmidt, H., Czeschel, R., and Visbeck, M. 2020b. Seasonal variability of the circulation in the Arabian Sea at intermediate depth and its link to the oxygen minimum zone. *Ocean Science, Discussion*, doi: 10.5194/os-2020-9.
- Schott, F. A. and McCreary, J. P.: The monsoon circulation of the Indian Ocean, *Progr. Oceanogr.*, 51 (1), 1–123, doi:10.1016/S0079-6611(01)00083-0, 2001.
- Schmechtig, C., Thierry, V., and the Bio Argo Team. 2015. Argo quality control manual for biogeochemical data. <http://dx.doi.org/10.13155/40879>.
- Shchepetkin, A. F., and McWilliams, J. C. 2003. A method for computing horizontal pressure-gradient force in an oceanic model with a nonaligned vertical coordinate, *J. Geophys. Res.*, 108(C3), 3090, doi:10.1029/2001JC001047.
- Shchepetkin, A. F., and McWilliams J. C. 2005. The Regional Ocean Modeling System: A split-explicit, free-surface, topography following coordinates ocean model, *Ocean Modell.*, 9, 347– 404.
- Shenoy, D.M., Suresh, I., Uskaikar, H., Kurain, S., Vidya, P.J., Shirodkar, G., Gauns, M.U., Naqvi, S.W.A. 2020. Variability of dissolved oxygen in the Arabian Sea Oxygen Minimum Zone and its driving mechanisms. *J. Mar. Syst.*, doi: 10.1016/j.jmarsys.2020.103310.
- Shulman, I., Kindle, J.C., DeRada, S., Anderson, S.C., Penta, B and Martin, P.J. 2004. Development of a hierarchy of nested models to study the California Current System. In *Estuarine and Coastal Modeling*, ed. L. Malcolm., and P.E. Spaulding, 74–88.
- Somayajulu, B.L.K., Sarin, M.M., and Ramesh, R. 1996. Denitrification in the eastern Arabian Sea: Evaluation of the role of continental margins using Ra isotopes. *Deep-Sea Res. II*, 43, 111-117.
- Song, Y. T., and Haidvogel, D. 1994. A semi-implicit ocean circulation model using a generalized topography-following coordinate system, *J. Comput. Phys.*, 115, 228–244.
- Stramski, D., Reynolds, R.A., Babin, M., Kaczmarek, S., Lewis, M.R., Rottgers, R., Sciandra, A., Stramska, M., Twardowski, M.S., Franz, B.A. and Claustre, H. 2008. Relationships between the surface concentration of particulate organic carbon and optical properties in the eastern South Pacific and eastern Atlantic Oceans. *Biogeosciences*, 5, 171-201.
- Sullivan, J.M., Twardowski, M.S., Zaneveld, J.R.V., Moore, C.C., 2013. Measuring optical backscattering in water. In: *Light Scattering Reviews. 7*. Springer-Praxis Books. Springer, Berlin Heidelberg, pp. 189–224.
- Takeshita, Y., Martz, T.R., Johnson, K.S., Plant, J.N., Gilbert, D., Riser, S.C., Neill, C., Tilbrook, B., 2013. A climatology-based quality control procedure for profiling float oxygen data. *J. Geophys. Res. Oceans* 118, 5640–5650. <https://doi.org/10.1002/jgrc.20399>.
- Thierry, V., Bittig, H. and the Argo-BGC team, 2018. Argo quality control manual for dissolved oxygen concentration, v2.0 <http://dx.doi.org/10.13155/46542>.

Thierry, V., Bittig, H. 2016. Argo quality control manual dissolved oxygen concentration, v1.1. <http://dx.doi.org/10.13155/46542>.

UdayBhaskar, T.V.S., Rao, E.P.R., Shesu, R.V., and Devender, R. 2012. A note on three way quality control of Argo temperature and salinity profiles – A semi-automated approach at INCOIS. *International J Earth Sciences and Engineering*, 5, 1510-1514.

Ullao, O., Canfield, D.E., DeLong, E.F., Letelier, R.M. and Stewart, F.J. 2012. Microbial oceanography of anoxic oxygen minimum zones. *Proceedings of Natl. Acad. Sci.*, 109, 15996-16003.

Wong, A., Keeley, R., Carval, T., and the Argo Data Management Team. 2020. Argo quality control manual for CTD and trajectory data. <http://dx/doi.org/10.13155/33951>.

Wilkin, J.L., Arango, H.G., Haidvogel, D.B., Lichtenwalner, C.S., Glenn, S.M. and Hedström, K.S., 2005. A regional ocean modeling system for the Long-term Ecosystem Observatory. *Journal of Geophysical Research: Oceans*, 110(C6).

Wojtasiewicz, B., Trull, T.W., Udaya Bhaskar, T.V.S., Gauns, M., Prakash, S., Ravichandran, M., Shenoy, D.M., Slawinski, D., Hardman-Mountford, N.J. 2018. Autonomous profiling float observations reveal the dynamics of deep biomass distributions in the denitrifying oxygen minimum zone of the Arabian Sea. *J. Mar. Syst.*, 207, 103103, 10.1016/j.jmarsys.2018.07.002.

Zhang, X., Hu, L., He, M.-X., 2009. Scattering by pure seawater: effect of salinity. *Opt.Express* 17, 5698–5710.

Legend to figures

- 1 A schematic representation of identified surface current flow during southwest monsoon (blue) and northeast monsoon (red). Currents indicated are WICC-West India Coastal Currents, GW-Great Whirl, RHJ-Ras al Hadd Jet, NEC-North Equatorial Current, and SEC-South Equatorial Current after Schott and McCreary (2001). The region of denitrification is shown as black line after Naqvi (1991). The regions of coastal upwelling are shown and brown line represents the Findlater Jet where open ocean upwelling occurs. The position of the Bio-Argo DO profiles used in this study are given as black dots. The classification of Arabian Sea with reference to different regions (NE, NW, SE, SW) are shown with dashed lines.
- 2 Spatial variations in a) upper boundary, b) lower boundary and c) thickness of the OMZ in the Arabian Sea where oxygen concentrations are $\sim 10 \mu\text{M}$. Red line shows the denitrification area.
- 3 Spatial variations in back-scatter (m^{-1}) a) along northeast-southwest transect (color shade) shown in (b). The dissolved oxygen concentrations are shown as contours. The position of the profiles are shown in the upper x-axis. b) distribution of back-scatter at the core of OMZ (300 m depth) in the Arabian Sea. Red line shows the denitrification area.
- 4 Spatial variations in a) depth of mixed layer (m) and b) integrated Chl-a in the upper 100 m in the Arabian Sea. Red line shows the denitrification area.
- 5 a) ROMS simulated monthly mean current for January, averaged for 2006–2017, at 300 m depth and b) ROMS simulated monthly mean current for July, averaged for 2006–2017, at 300 m depth. Colour shading shows the magnitude of currents (m/s) while the vectors (of fixed length) show the direction of the currents. Black line shows the denitrification area.
- 6 Spatial variations in a) temperature ($^{\circ}\text{C}$), b) salinity and c) dissolved oxygen (μM) at the core of OMZ (depth of 300m) in the Arabian Sea. Red line shows the denitrification area.
- 7 Spatial variations in a) depth integrated primary production in the photic zone ($\text{mgC m}^{-2} \text{d}^{-1}$) (from Bhattathiri et al., 1996; Barber et al., 2001; Sarma and Dalabehera, 2019) and d) sinking carbon fluxes at 100 m depth ($\text{mgC m}^{-2} \text{d}^{-1}$) in the Arabian Sea (from Buesseler et al., 1998; Anand et al., 2018).

Figure 1:

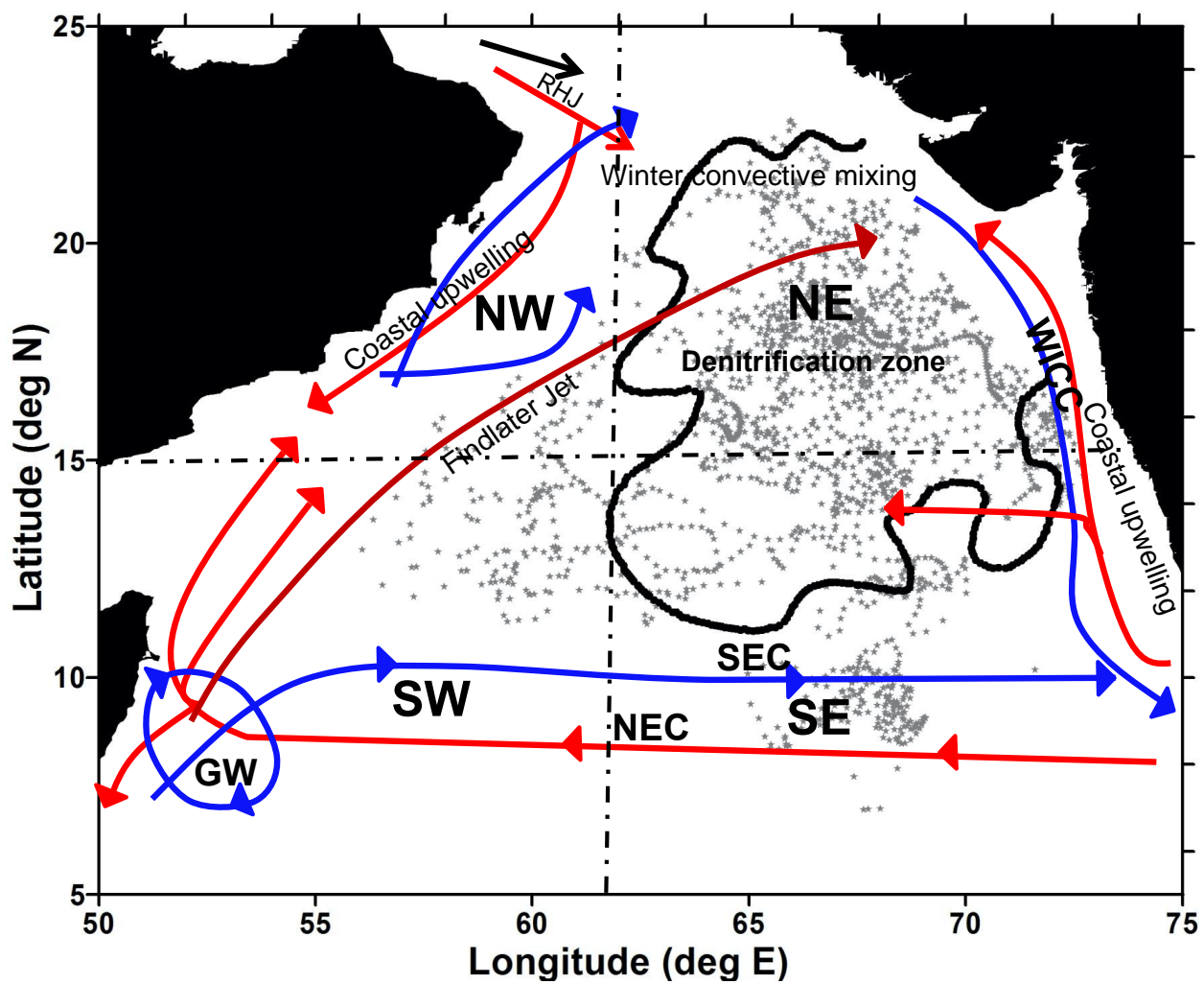


Figure 2:

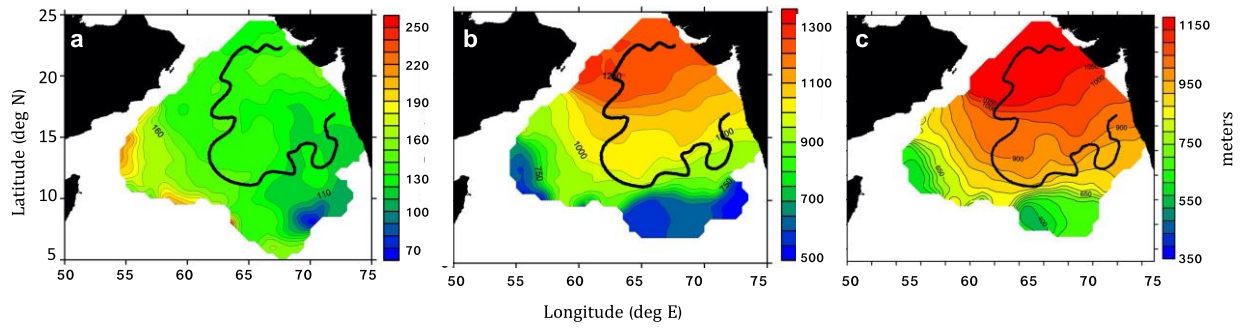


Figure 3:

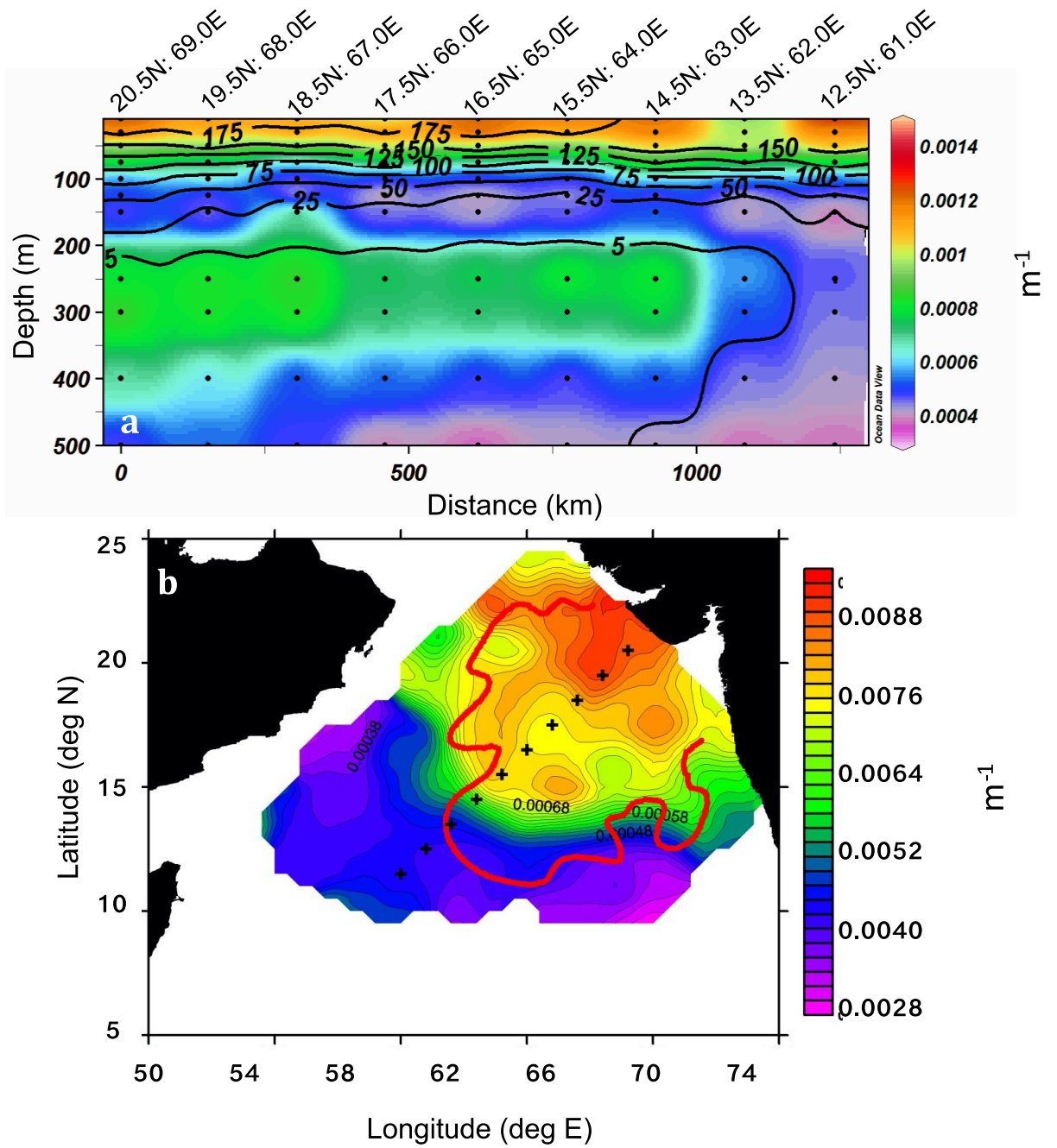


Figure 4:

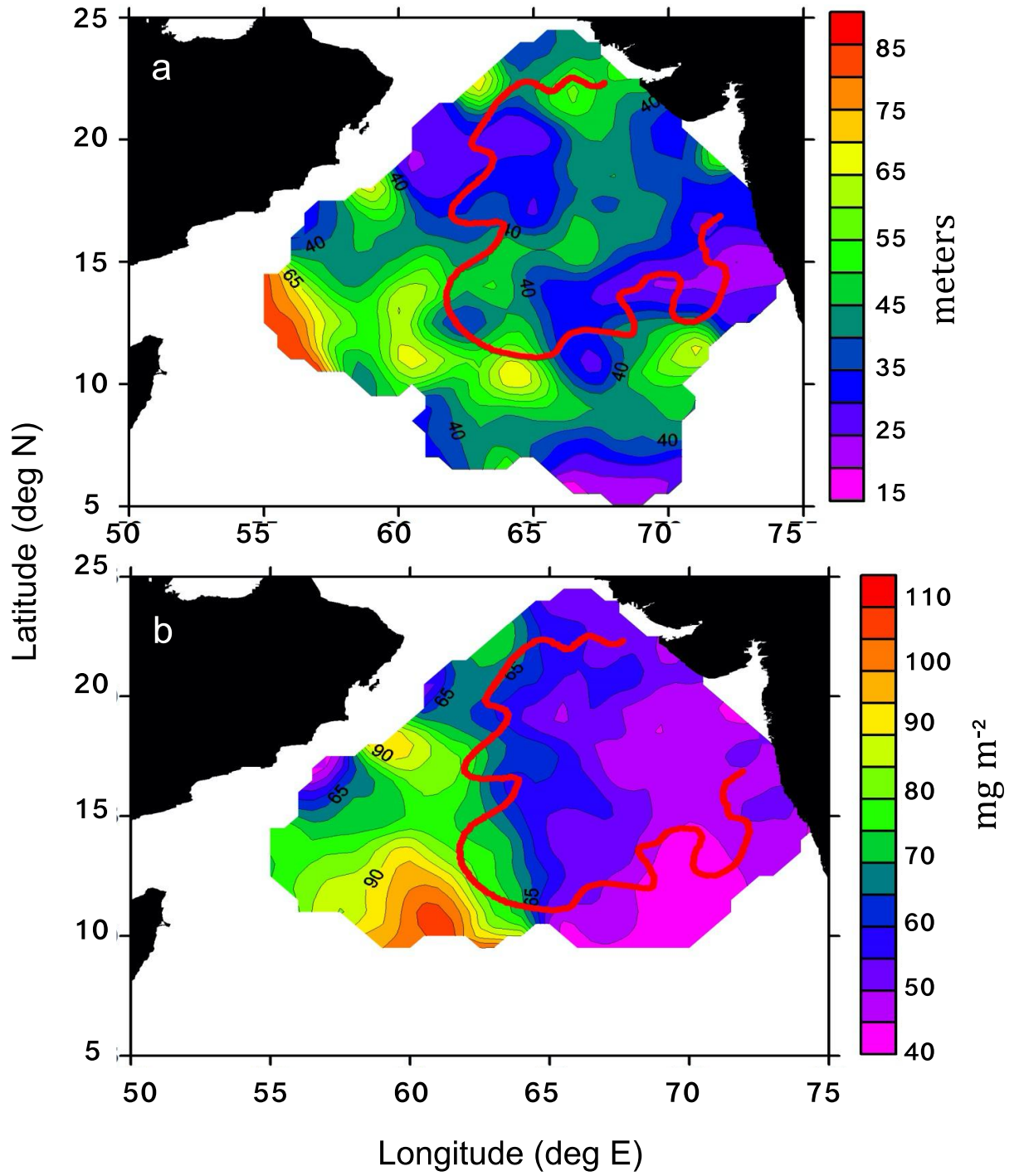


Figure 5:

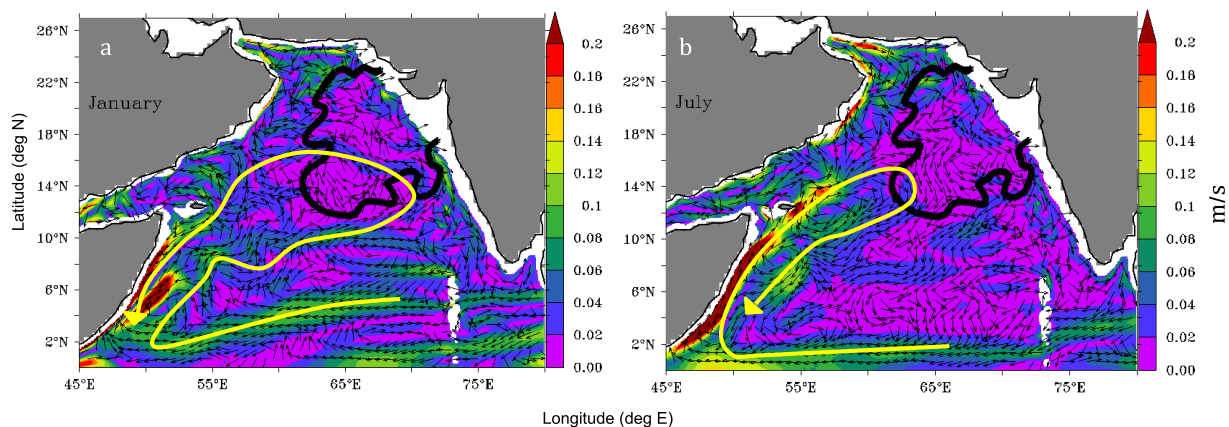


Figure 6:

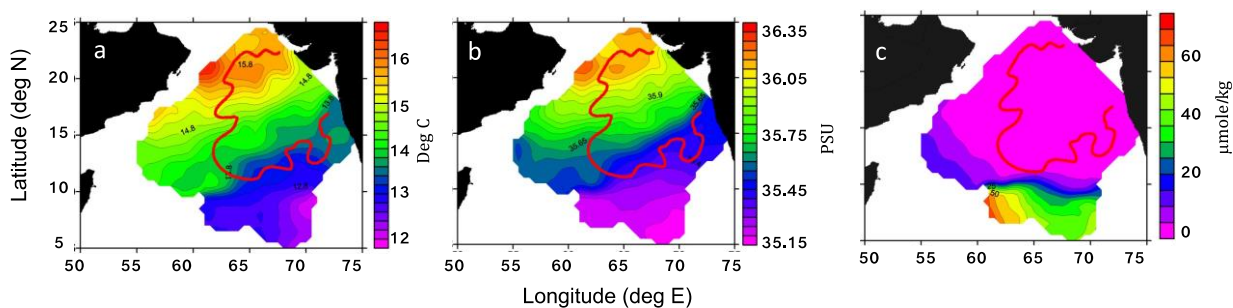


Figure 7:

